Hollow Urchin-like ZnO thin Films by Electrochemical Deposition

By *Jamil Elias,* Claude Lévy-Clément, Mikhael Bechelany, Johann Michler, Guillaume-Yangshu Wang, Zhao Wang,* and *Laetitia Philippe*

Since the first report on ultraviolet lasing from ZnO nanowires (NWs),[1] remarkable effort has been dedicated to the development of novel synthesis routes for 1D ZnO nanostructures. Ordered arrays of 1D ZnO NWs have a promising future as applications in electronic and optoelectronic devices, because they are expected to improve the performance of various nanodevices such as short-wavelength lasers,[1] nanostructured solar cells,[2,3] electroluminescent,[4] and field-emission devices.[5] What is now a relevant area of focus in nanoscience involves the preparation of higher-order assemblies, arrays, and superlattices of these 1D nanostructures.[6] Recently, many efforts have focused on the integration of 1D nanoscale building blocks into 3D architectures. Hollow urchin-like ZnO NWs that combine properties of 3D and 1D materials may emerge as a more interesting alternative than simple arrays of NWs due to the higher specific surface and porosity,[7] especially for application in dye and semiconductor-sensitized solar cells.[3,8] To date, there are only two strategies to synthesize hollow urchin-like ZnO NWs. The first one[9] is a wet-chemical route that uses a modified Kirkendall process, by which zinc powders that are spherical in shape are transformed into hollow urchin-like ZnO NWs dispersed in solution. The second strategy[10–12] is based on the calcination of metallic Zn microsphere powders at relatively high temperature (500–750 °C). With these two approaches, ZnO nanostructures are often randomly distributed (in size and organization), which may limit their practical applications as building blocks in nanodevices. Nevertheless, it is essential for the fabrication of nanodevices to assemble NW-structured hollow spheres with a uniform size in ordered arrays, since such an organisation combines the merits of patterned arrays and nanometer-sized materials. Until now, a suitable technique is still missing for the fabrication of ordered arrays of hollow urchin-like ZnO NWs with tunable sizes.

In this paper, we report on a novel approach to fabricate well-ordered hollow urchin-like single-crystal ZnO NWs with controlled NW and core dimensions. The method combines the formation of a polystyrene (PS) microsphere colloidal mono/multilayer and the electrodeposition of ZnO NWs, followed by the elimination of the PS microspheres, which play the role of a template. It is shown that the light scattering properties of such an ordered architecture exceed those of ZnO NW arrays. Applications as 3D building blocks in the field of nanostructured solar cells are discussed.

Mono/multilayers of PS spheres covering conductive substrates have been used as templates to electrodeposit inverse opal structures.[13,14] In such cases the nucleation of ZnO took place at the interstitial sites (on a conductive substrate) between the PS spheres leading to different morphologies depending on the employed method. Our strategy of electrodeposition differs from those previously described by the mode of nucleation and growth. In our case, the deposition of ZnO takes place, from the nucleation step, on the PS spheres and the conductive substrate, simultaneously. As a result, the spheres are homogenously covered by a thin film composed of single-crystal ZnO NWs connected together at their base. This approach provides a simple and versatile way to synthesize well-ordered mono/multilayers of ZnO hollow microspheres with the ability to control the sphere size in addition to the ZnO NW dimensions and morphology.

A monolayer of commercially available carboxylate-modified PS spheres (~4.3 μm) is deposited directly on a transparent conductive oxide (TCO) substrate by using a self-assembly technique on a water surface. We have used the method of Zhou et al.[14] with some modifications. A detailed description of our process is given in the experimental section. Figure 1a shows a tilted, low-magnification scanning electron microscopy (SEM) image of the self-assembled monolayer on TCO substrate. A well-organized monolayer of PS microspheres can be observed in addition to occasional point defects in some regions due to the presence of larger spheres in the commercial solution (circled region in Fig. 1a). This organization is observed throughout the entire TCO surface (~1.5 cm^2). As a proof of that, the lower inset in Figure 1a shows an optical image of TCO/PS where the sample colour is perfectly homogeneous, reflecting the presence of only one PS domain (monolayer) on the substrate. The detailed organization of the spheres was investigated by a closer examination using high-magnification SEM (Fig. 1b and its inset), which shows a relatively large area of the self-assembled monolayer and a perfectly ordered array. The TCO/PS sample has then been immersed for 30 min in 2 M $ZnCl_2$ aqueous solution at room temperature and used as a working electrode in an electrochemical cell for the deposition of ZnO NWs. The electrolyte was an aqueous solution saturated by molecular O_2, containing 5×10^{-4} M $ZnCl_2$ (zinc precursor) and 0.1 M KCl

---

[*] Dr. J. Elias, Dr. M. Bechelany, Dr. J. Michler, Dr. Z. Wang, Dr. L. Philippe
Laboratory for Mechanics of Materials and Nanostructures
Empa Materials Science and Technology
Feuerwerkstrasse 39, 3602 Thun, Switzerland
E-mail: jamil.elias@empa.ch

Prof. C. Lévy-Clément, Dr. G.-Y. Wang
Institut de Chimie et Matériaux de Paris-Est, CNRS, UMR 7182
2-8 rue Henri Dunant, 94320 Thiais Cedex, France

DOI: 10.1002/adma.200903098

© 2010 WILEY-VCH Verlag GmbH & Co. KGaA, Weinheim

WILEY InterScience® DISCOVER SOMETHING GREAT

Final page numbers not assigned

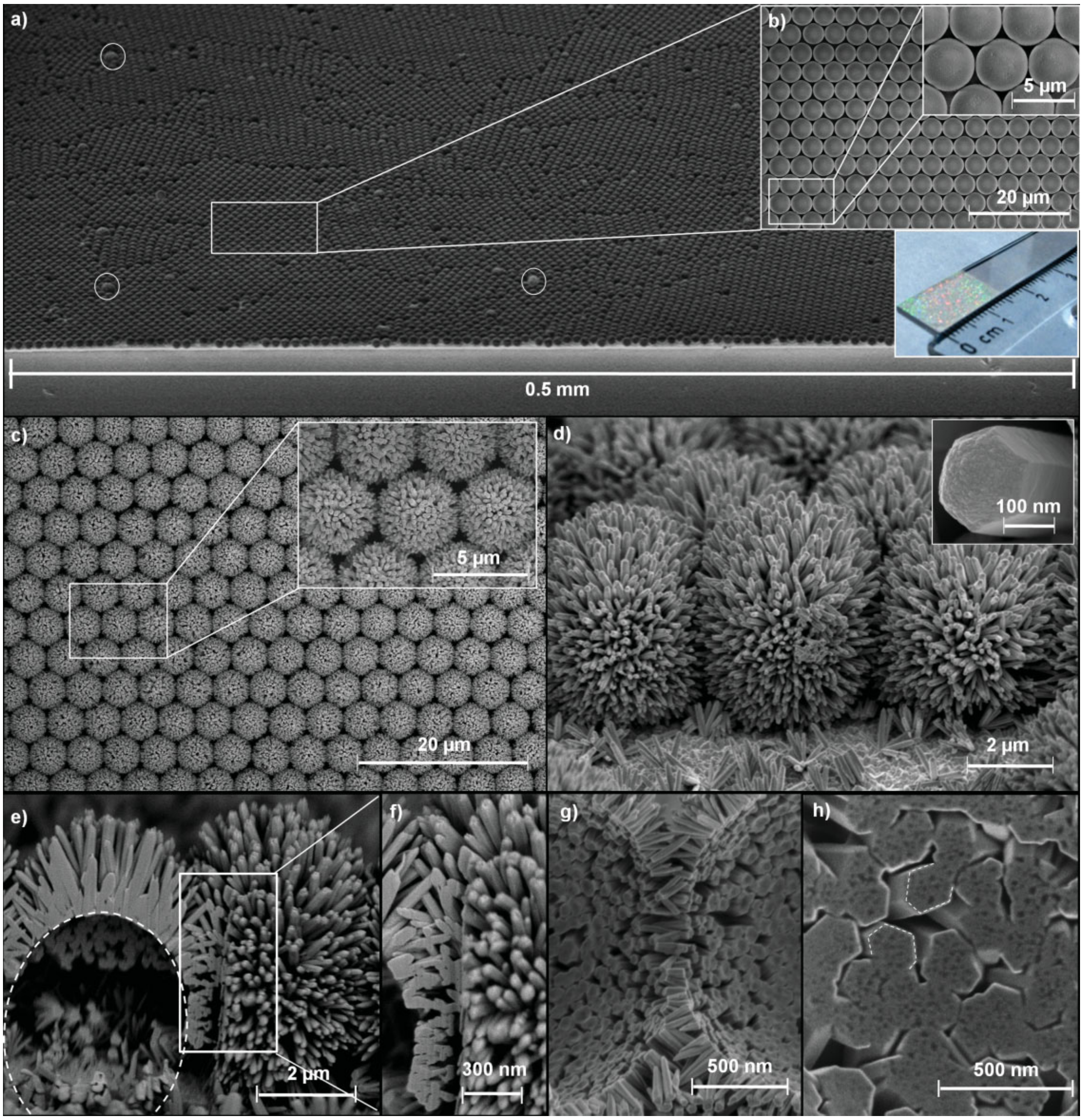

Figure 1. a,b) SEM images of a self-assembled monolayer of PS microspheres on a TCO substrate; a) tilted (45°) low magnification and b) top view. The lower inset of (a) presents the digital image of the same sample. c,d) SEM images of an ordered hollow urchin-like structure of ZnO nanowires after the removal of PS; c) top view, the inset is a higher magnification, and d) tilted view (70°). The inset is a high-magnification SEM image of the top of a nanowire grown at the top of the urchin-like structure. e,f) Cross-sectional SEM images of two urchin-like structures treated by FIB at different magnifications. g,h) High-magnification SEM images of a mechanically scratched structure for cross-section and internal surface observations, respectively.

(supporting electrolyte). The temperature was maintained at 80 °C. The electrodeposition of ZnO was performed at constant potential (−1 V) with a 15 C/cm^2 charge density. Figures 1c and 1d depict the top- and tilted-view SEM images of the prepared sample after the removal of PS (dissolved in toluene or burned off). The top view (Fig. 1c) shows the formation of groups of freestanding NWs uniformly assembled into an array. All groups exhibit an urchin-like shape. At higher magnification the diameters of the urchin-like structures and their NWs are uniform with average values of ~4.3 µm and ~220 nm, respectively. It is worthy to note that without the treatment in the 2 M $ZnCl_2$ solution, the NWs are deposited only on TCO between the PS spheres and not on the spheres. It can be clearly seen in the tilted view (close to a scratched part of the sample, Fig. 1d) that the ZnO structures have an elliptical morphology. They are close-packed, comprise a high density of hexagonal NWs (see inset of Fig. 1d) grown perpendicular to the original PS surface, and exhibit a highly developed surface area. In addition, well-aligned and freestanding NWs are observed on the TCO substrate between the urchin-like structures, increasing even more the surface area. These results raise important questions, such as why urchin-like structures with lateral diameter roughly similar (~ 4.3 µm) to that of close-packed PS have been obtained (Fig. 1b) and how can the ZnO NWs grow between two closely adjusted PS spheres? Answers might be given by investigating the core of a hollow urchin-like structure and the interface

WILEY InterScience® DISCOVER SOMETHING GREAT
© 2010 WILEY-VCH Verlag GmbH & Co. KGaA, Weinheim

between two close-packed spheres. Focused ion beam (FIB) milling was used in order to cut the hollow urchin-like structures. The cutting was carried out orthogonally to the TCO substrate at the center of the structures. Two resulting structures close to each other are shown in Figure 1e. The left-side structure is completely hollow although the lower part has fallen down because of the FIB processing. Since all the structures in the sample have been subjected to the same treatment for removing the PS spheres, the structure on the right is then expected to be hollow inside. This was confirmed by energy dispersive X-ray (EDX) analyses carried out on a structure before and after removing the PS (Fig. 3a). The disappearance of the carbon peak is indeed observed after removal of the PS spheres. The left-side structure in Figure 1e also shows that the ZnO NW-shell has different thicknesses, increasing gradually from the bottom to the top of the sphere where the NWs length reaches 600 nm. The interface between these two structures depicted in the high magnification image of Figure 1f shows that the NWs grown on the sides between the two closed-packed spheres are interlaced, and exhibit a minimum length of ~225 nm at the original contact point of the two PS spheres. Though the initial morphology of PS before the deposition of ZnO was spherical, after this deposition and PS elimination the structures evolved into an ellipsoidal shape as shown by the dashed line in Figure 1f. This means that a deformation of the PS spheres takes place during the growth process of ZnO, explaining that a similar diameter is observed for PS spheres and PS/ZnO urchins, in the top-view images (Fig. 1b and 1c, respectively). Since the stiffness of PS is more than 50 times lower than that of ZnO (~3.3 GPa compared to ~180 GPa),[15] the deformation of the PS spheres could be due to the internal stress induced at the ZnO/PS interface and the repulsive force given by ZnO NWs growing against each other. A finite element simulation has been performed and confirms the possibility of such deformation from a mechanical point of view (see the movie S1 in the Supporting Information). The cross section and the internal surface of these structures can be observed in detail on mechanically scratched structures in Figures 1g and 1h, respectively. The two broken structures attached to each other at the interface (Fig. 1g) show that the ZnO NWs with a perfect hexagonally faceted morphology are pointing toward the center of the urchin structures. The internal surface in Figure 1h shows more clearly the hexagonal shape (dashed lines) at the bottom of the interconnected NWs.

In order to gain further insight into the growth process of ZnO NWs on PS microspheres, the evolution of both the morphology and the dimensions of ZnO nanostructures as a function of the charge density (i.e., time of deposition) were studied by SEM and the results are summarized in Figure 2. The charge density was varied from 0.5 to 25 C/cm^2. Small ZnO nanocrystal particles partially and homogenously covering the PS spheres are observed at 0.5 C/cm^2 in the SEM top view of Figure 2a. A tilted view of this sample confirms that these nanocrystals uniformly cover the surface of the PS spheres (Fig. 2b). In addition, a high magnification image (inset of Fig. 2b) shows that similar ZnO nanocrystal particles are also deposited onto TCO (arrows) between the PS. This reveals that the electrodeposition of ZnO follows the same nucleation and growth mechanism on both surfaces (PS and TCO). Figure 2c displays the SEM top view image of the electrodeposit obtained at 5 C/cm^2, showing that the small nanocrystals (obtained at 0.5 C/cm^2 in Fig. 2a) increase in size and are transformed into nanorods, that still do not completely cover the PS surface. After passing 25 C/cm^2, the diameter and the length of nanorods increase even more, and the nanorods coalesce at their bottom, forming a dense NW network completely covering the surface of the PS spheres (Fig. 2d).

The above results and the formation of hollow urchin-like ZnO NWs can be interpreted by the process summarized in Scheme 1. We suggest that the key point for the formation of the ZnO/PS composite is the interaction between the carboxylate groups of the PS microspheres and the zinc precursor. Preceding the electrodeposition and after treatment in an aqueous solution of $ZnCl_2$ (2 M), Zn^{2+} ions interact and bind with the carboxylate groups (Scheme 1a) of PS and adsorb on their surface (Scheme 1b). This adsorption is confirmed by EDX measurements that were carried out before and after the treatment (Fig. 3b), with the appearance of a small Zn peak in the spectrum after Zn^{2+} adsorption. The conditions (room temperature and 2 M $ZnCl_2$) employed in this step of the process are crucial in order to adsorb the highest amount of Zn^{2+} ions on the active carboxylate sites of PS. Although the electrodeposition solution contains the same zinc precursor (5×10^{-4} M $ZnCl_2$), both concentration and temperature play a major role in this step. Goux et al.[16] reported a thermochemical analysis of $ZnCl_2$ decomposition in aqueous solutions. They showed that the major soluble species at room temperature is Zn^{2+} (>80%), which

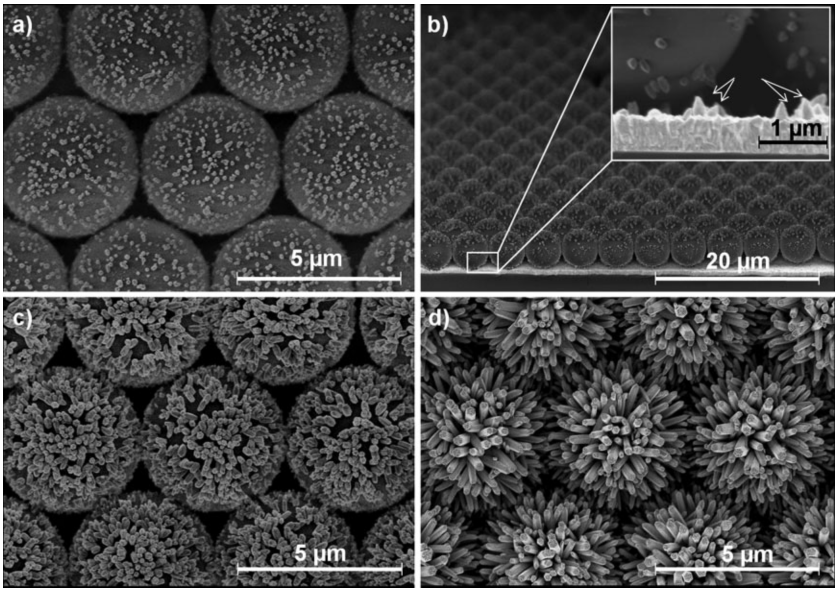

Figure 2. a,c,d) Top view SEM images of ZnO deposited on PS with a 0.5, 5, and 25 C/cm^2 charge density, respectively. We note that the PS spheres are removed in (d). b) Tilted (45°) SEM view of (a). The inset is a cross-sectional high-magnification SEM image of (b).

© 2010 WILEY-VCH Verlag GmbH & Co. KGaA, Weinheim

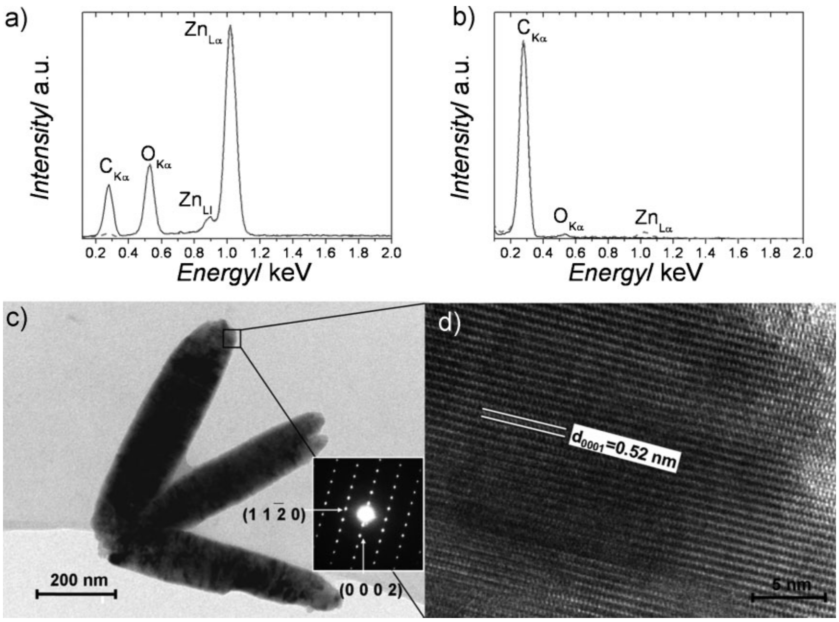

Figure 3. a) EDX spectra of an urchin-like ZnO NWs structure before (black solid) and after (red dashed) dissolution of PS. b) EDX spectra of PS sphere before (black solid) and after (red dashed) treatment in 2 M $ZnCl_2$. Before the measurements, the samples were washed with distilled water. c) Bright field TEM image of three interconnected ZnO nanowires scratched from an urchin-like structure and obtained with the same conditions than those of Figure. 1c. d) High-resolution TEM image of the selected area in Fig. c). The inset is the electron diffraction pattern of the left nanowire.

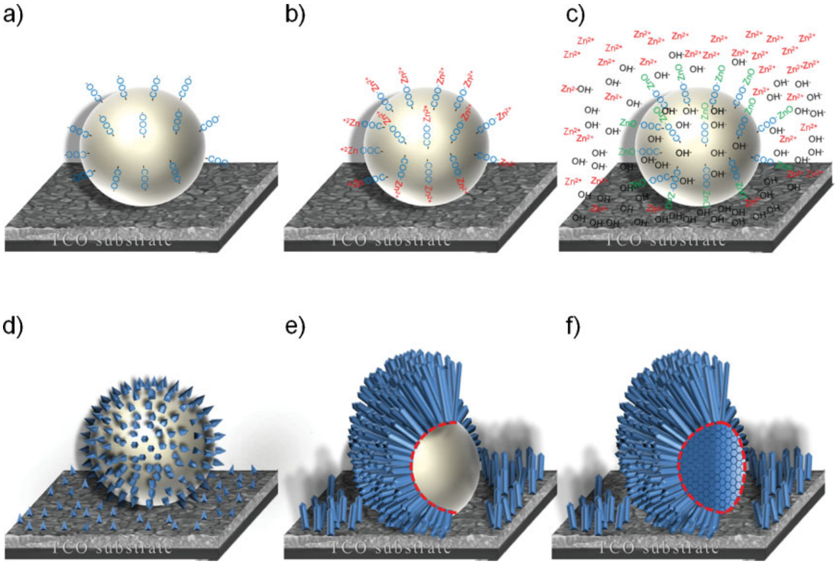

Scheme 1. Schematic view of the fabrication processes of hollow urchin-like ZnO NWs. a) Carboxylate-modified PS sphere deposited on TCO substrate. b) After treatment in 2 M $ZnCl_2$ aqueous solution and reaction between the carboxylate terminal and Zn^{2+}. c) Repartition of the species around the treated PS, in the electrodeposition solution and formation of ZnO nuclei (green). d) First growth stage of ZnO nanocrystals on PS and TCO substrate. e) Cross section PS/ZnO showing the growth of base-interconnected and free-standing NWs on PS and TCO substrate, respectively. f) Cross section of the hollow urchin-like ZnO structure after the removal of PS.

decreases to less than 20% at 90 °C (close to the electrodeposition temperature of ZnO NWs). In order to obtain a conductive polystyrene layer, the TCO/PS was treated before the electrochemical deposition with a relatively high $ZnCl_2$ concentration at room temperature. Experimentally, we have observed that when the $ZnCl_2$ concentration is lower than 2 M, the density of electrodeposited ZnO nanocrystals on PS is relatively low and only separated NWs that do not cover the entire surface of PS are deposited (Fig. S2 in the Supporting Information). According to Peulon and Lincot[17] the electrodeposition of ZnO occurs from the reduction of molecular O_2 in presence of a zinc precursor. By applying a cathodic potential, hydroxide ions (Eq. (1)) are electrochemically generated at the electrode surface (e.g. TCO), leading to the precipitation of ZnO (Eq. (2)).

$$O_2 + 2H_2O + 4e^- \rightarrow 4OH^- \qquad (1)$$

$$Zn^{2+} + 2OH^- \rightarrow ZnO + H_2O \qquad (2)$$

This mechanism is shown in Scheme 1c with the presence of the modified PS onto the substrate. Once the OH^- ions are generated at the electrode, they subsequently interact with zinc cations adsorbed on the PS surface to produce nuclei of ZnO (Eq. (2)) on the active sites of the sphere. The nucleation process is followed by the growth of the nuclei by the reaction between the electrogenerated OH^- and Zn^{2+} diffusing from the solution. Afterwards, the growth of ZnO occurs during a short time period on TCO and the PS sphere to produce small nanocrystals, as illustrated in Scheme 1d. These nanocrystals continue growing and evolve into freestanding NW arrays on TCO and base-interconnected NWs on PS (Scheme 1e). As shown in the cross section of Figure 1e, the NWs length increases gradually from the bottom to the top of PS spheres. This is attributed to the fact that the Zn^{2+} ions react (Eq. (2)) more easily on the most accessible NWs[18b] located at the upper part of PS, lowering gradually the growth rate of ZnO at the bottom of the sphere. This process is the same for a randomly distributed array where the structures are separated from each other (See Fig. S3 in the Supporting Information). Finally, the PS sphere is removed and a hollow urchin-like shell of ZnO NWs is obtained (Scheme 1f).

In previous work,[18] we have successfully electrodeposited large-scale 1D ZnO arrays with controlled dimensions and morphologies (e.g. NWs, nanoneedles, nanotubes, etc.) on

WILEY InterScience DISCOVER SOMETHING GREAT
© 2010 WILEY-VCH Verlag GmbH & Co. KGaA, Weinheim

TCO substrate by varying different electrochemical parameters. Since the mechanism of deposition is demonstrated (Scheme 1d and Fig. 2b) to be similar on TCO and PS, the electrodeposition parameters previously determined,[18] should also be valid on TCO/PS electrode. As a proof, ZnO NWs in the urchin-like structure have been obtained with different dimensions by only adjusting the concentration of $ZnCl_2$ and KCl (Fig. S4 in the Supporting Information).[18] More interestingly, multilayered structures of hollow urchin-like ZnO NWs could be obtained (Fig. S5 in the Supporting Information) by following the same process described above, but repeating the first step (deposition of a PS monolayer) as a function of the desired number of monolayers.

The crystalline structure of the electrodeposited ZnO has been studied by transmission electron microscopy (TEM). Figure 3d shows a high-resolution TEM image of the top of a single NW from an urchin-like structure (square of Figure 3c). Crystal planes aligned perpendicularly to the growth direction are clearly visible. The measured inter-plane spacing (0.52 nm) matches well with the literature value for planes such as (0001) in wurtzite ZnO, showing that the NWs grow along the [0001] direction. The associated selected area electron diffraction (SAED) pattern (inset of Figure 3c) confirms that ZnO NWs are single crystals.

Our new approach has enabled us to produce a wide range of ordered urchin ZnO NWs on relatively large surfaces of TCO. We expect that these structures will be useful in many applications and nanodevices. As preliminary experiments, we investigated the geometry influence on solar light scattering. The spectral dependence of the reflectance was analyzed and compared to a typical array of ZnO NWs roughly of the same dimensions as those present in the urchin-like structure. A spectacular increase (more than 50%) of the reflectance (Fig. 4) was observed throughout the entire visible wavelength range by comparing NW arrays with the ordered hollow urchin-like structures. In addition, both spectra show UV absorbance edges close to 375 nm ($Eg = 3.3$ eV), which corresponds to the band-gap energy of ZnO.[19] Recently, we have demonstrated that the size[20] and the morphology[21] of 1D ZnO play important roles for controlling the light scattering. For photovoltaic applications in semiconductor sensitized solar cells, ZnO NWs can be for example conformally lined with an extremely thin layer (10–30 nm thick) of CdSe, absorbing light at 1.73 eV. A 10 nm thick CdSe layer was successfully electrodeposited on ZnO NWs giving ZnO/CdSe urchins (Fig. S6 in the Supporting Information). A clear correlation between the light scattering in ZnO arrays and the light absorption in ZnO/CdSe urchin-like heterostructures has been found. Consequently, this new architecture can be also sensitized to solar light and used as more efficient building-blocks for different types of nanostructured solar cells.

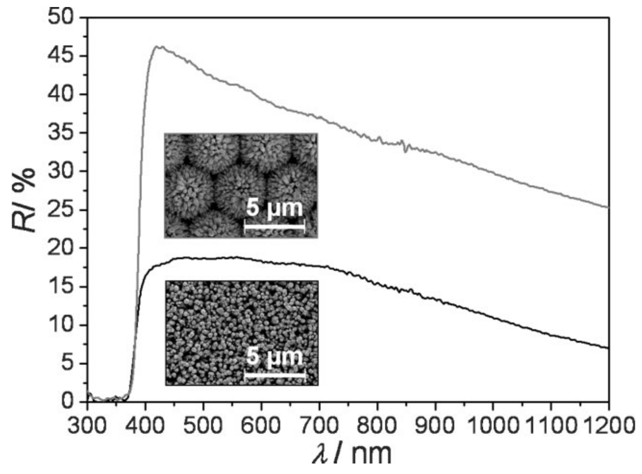

Figure 4. Total reflectance spectra of glass/SnO_2:F/ZnO free-standing nanowires sample (black) and ordered hollow urchin-like structures (red) array. The nanowires' dimensions are similar for both samples. Each SEM image corresponds to its spectrum above.

In summary, we have developed a novel low-cost method to produce large area of single crystal and perfectly-ordered hollow urchin-like ZnO NW arrays by a combined colloidal patterning and electrochemical approach at temperature as low as 80 °C. The process enables a versatile control of dimensions and morphologies of ZnO NWs as well as control of the core diameter and spatial arrangement (by changing the size of PS spheres) for the first time. The key mechanism for the formation of these architectures is the treatment of PS with $ZnCl_2$ at high concentration which renders them electrically conductive, enabling the deposition of ZnO on their surface. This mechanism opens up new opportunities for processing novel metal oxide or hydroxide materials based on a similar growth mechanisms[22] to that of ZnO (e.g. CdO,[23] TiO_2,[24] CeO_2,[25] $Co(OH)_2$,[26] $Ni(OH)_2$,[27] etc.). Importantly, preliminary experiments have confirmed a strong improvement of light scattering by the urchin-like ZnO NW thin films, offering promising applications as building-blocks in different types of nanostructured solar cells (organic, hybrid and dye sensitized solar cells) and potentially useful for a wide variety of applications in optical devices, photonic crystals, and nanodevices.

Experimental

Commercially available Carboxylate-modified PS microspheres suspension (Ø ∼ 4.3 and 3 μm, 4 wt% aqueous dispersion) were bought from Duke Scientific U.S.A and used as received. The substrates were commercial TCO (glass/SnO_2:F, 10 Ω/sq.) from Solaronix Company, Switzerland. The bare TCO were cleaned thoroughly by sonication in acetone, ethanol and isopropanol, consecutively, for 15 min each. 300 μL of a carboxylate-modified PS microsphere suspension was diluted with an equal volume of ethanol and dispersed (drop-by-drop using a micropipet) onto the surface of deionized water in an 8-cm diameter Petri dish. After the self-assembling process of PS on the water surface, the TCO substrate (1 cm × 5 cm) tilted (45°) was immersed partially (e.g., 1.5 cm^2) and vertically into the solution. Subsequently, the monolayer of PS was transferred slowly onto the TCO substrate during the removal from the solution, by keeping the same angle (45°). After drying, TCO substrate covered with PS was heated in an oven (at 100 °C for 10 min) to sinter the PS and adhere it to the substrate. TCO/PS sample was then immersed (for 30 min) under a low agitation in an aqueous solution of $ZnCl_2$ (2 M) at room temperature. After being rinsed with distilled water, the treated sample was then used as a working electrode in a three-electrode electrochemical cell, with Pt spiral wire as the counter electrode and a saturated calomel electrode (SCE) as the reference electrode. The electrolyte was an aqueous solution saturated by molecular O_2 and containing zinc chloride (5×10^{-4} M, zinc precursor) and potassium chloride (0.1 M, supporting electrolyte). The electrodeposition was performed at a constant electric potential (−1 V) and the charge density was varied between 0.5 to 25 C/cm^2 using an Autolab PGSTAT-30 potentiostat. After electrodeposition, PS microspheres were dissolved in toluene or burned off in air at 450 °C for 1 h.

© 2010 WILEY-VCH Verlag GmbH & Co. KGaA, Weinheim

The CdSe coating was electrodeposited following the method published in Reference [28].

The morphology of the samples was observed with scanning electron microscopy (SEM, Hitachi S-4800). The structural properties were analyzed by transmission electron microscopy (TEM) using high-resolution mode (Tecnai F20 FEG at 200 kV). A drop of an ethanol suspension containing the ZnO nanostructures was deposited on a copper grid with lacey carbon for TEM observations. The cutting of ZnO structures was carried out by using a Lyra dual beam FIB from Tescan. A liquid ion metal source (LIMS) of Gallium with an acceleration voltage of 30kV was used. The sample was perpendicular to the ion gun resulting in a 55° tilt to the electron gun. The energy dispersive X-ray (EDX) spectrum was obtained with a Genesis 4000 EDAX in SEM. The optical reflectivity (*R*) was measured at room temperature with a Hitachi UV-VIS-NIR 4001 spectrophotometer fitted with an integrating sphere, from 300 to 1200 nm.

Acknowledgements

The authors thank Dr. William Mook for valuable discussions and Gerhard Buerki for FIB experiments. This work was supported by SFOE (Swiss Federal Office for Energy) ETA Solar Cell project, No. 103296, Switzerland. Supporting Information is available online from Wiley InterScience or from the author.

Received: September 8, 2009
Revised: October 27, 2009
Published online:

---

[1] M. H. Huang, S. Mao, H. Feick, H. Yan, Y. Wu, H. Kind, E. Weber, R. Russo, P. Yang, *Science.* **2001**, *292*, 1897.
[2] G. Boschloo, T. Edvinsson, A. Hagfeldt, in Nanostructured Materials for Solar Energy Conversion, (Ed. T. Soga), Elsevier, **2006**, pp. 227–254.
[3] C. Lévy-Clément, A. Hagfeldt, in *Nanostructured Materials for Solar Energy Conversion*, (Ed. T. Soga), Elsevier, **2006**, pp. 444–484.
[4] W. I. Park, G. C. Yi, *Adv. Mater.* **2004**, *16*, 87.
[5] Y. K. Tseng, C. J. Huang, H. M. Cheng, I. N. Lin, K. S. Liu, I. C. Chen, *Adv. Funct. Mater.* **2003**, *13*, 811.
[6] H. J. Fan, P. Werner, M. Zacharias, *Small*, **2006**, *2*, 700.
[7] X. W. Lou, L. A. Archer, Z. Yang, *Adv. Mater.* **2008**, *20*, 3987.
[8] I. Gonzalez-Valls, M. Lira-Cantu, *Energy Environ. Sci.* **2009**, *2*, 19.
[9] B. Liu, H. C. Zeng, *J. Am. Chem. Soc.* **2004**, *126*, 16744.
[10] G. Shen, Y. Bando, C. J. Lee, *J. Phys. Chem. B* **2005**, *109*, 10578.
[11] X. Wang, P. Hu, Y. Fangli, L. Yu, *J. Phys. Chem. C* **2007**, *111*, 6706.
[12] Z. Gu, M. P. Paranthaman, J. Xu, Z. W. Pan, *ACS Nano* **2009**, *3*, 273.
[13] a) B. Cao, W. Cai, F. Sun, Y. Li, Y. Lei, L. Zhang, *Chem. Commun.* **2004**, *14*, 1604. b) H. Yan, Y. Yang, Z. Fu, B. Yang, L. Xia, S. Fu, F. Li. *Electrochem. Commun.* **2005**, *7*, 1117. c) M. Fu, J. Zhou, Q. Xiao, B. Li, R. Zong, W. Chen, J. Zhang, *Adv. Mater.* **2006**, *18*, 1001. d) L. K. Teh, K. H. Yeo, C. C. Wong, *Appl. Phys. Lett.* **2006**, *89*, 051105.
[14] Q. Zhou, J. Zhao, W. Xu, H. Zhao, Y. Wu, J. Zheng, *J. Phys. Chem. C* **2008**, *112*, 2378.
[15] a) K. Miyake, N. Satomi, S. Sasaki, *Appl. Phys. Lett.* **2006**, *89*, 031925. b) C. Chen, Y. Shi, Y. Zhang, J. Zhu, Y. Yan, *Phys. Rev. Lett.* **2006**, *96*, 075505.
[16] A. Goux, T. Pauporté, J. Chivot, D. Lincot, *Electrochim. Acta* **2005**, *50*, 2239.
[17] a) S. Peulon, D. Lincot, *Adv. Mater.* **1996**, *8*, 166. b) S. Peulon, D. Lincot, *J. Electrochem. Soc.* **1998**, *145*, 864.
[18] a) R. Tena-Zaera, J. Elias, G. Wang, C. Lévy-Clément, *J. Phys. Chem. C* **2007**, *111*, 16706. b) J. Elias, R. Tena-Zaera, C. Lévy-Clément, *J. Electroanal. Chem.* **2008**, *621*, 171. c) J. Elias, R. Tena-Zaera, G. W. Wang, C. Lévy-Clément, *Chem. Mater.* **2008**, *20*, 6633.
[19] V. Srikant, D. R. Clarke, *Appl. Phys. Lett.* **1998**, *10*, 5447.
[20] R. Tena-Zaera, J. Elias, C. Lévy-Clément, *Appl. Phys. Lett.* **2008**, *93*, 233119.
[21] C. Lévy-Clément, J. Elias, R. Tena-Zaera, *Phys. Status Solidi C* **2009**, *7*, 1596.
[22] G. H. Therese, P. V. Kamath, *Chem. Mater.* **2000**, *12*, 1195.
[23] A. Seshadri, N. R. de Tacconi, C. R. Chenthamarakshan, K. Rajeshwar, *Electrochem. Solid-State Lett.* **2006**, *9*, C1.
[24] C. Natarajan, G. Nogami, *J. Electrochem. Soc.* **1996**, *143*, 1547.
[25] a) F. B. Li, R. C. Newman, G. E. Thompson, *Electrochim. Acta* **1997**, *42*, 2455. b) S. A. Hayes, P. Yu, T. J. O'Keefe, M. J. O'Keefe, J. O. Stoffer, *J. Electrochem. Soc.* **2002**, *149*, C623. L. Gonzalez-Rovira, J. M. Sanchez-Amaya, M. Lopez-Haro, E. del Rio, A. B. Hungria, P. Midgley, J. J. Calvino, S. Bernal, F. J. Botana, *Nano Lett.* **2009**, *9*, 1395.
[26] S. P. Jiang, C. Q. Cui, A. C. C. Tseung, *J. Electrochem. Soc.* **2002**, *138*, 3599.
[27] C. C. Streinz, A. P. Hartman, S. Motupally, J. W. Weidner, *J. Electrochem. Soc.* **1995**, *142*, 1084.
[28] C. Lévy-Clément, R. Tena-Zaera, M. A. Ryan, A. Katty, G. Hodes, *Adv. Mater.* **2005**, *17*, 1512.

© 2010 WILEY-VCH Verlag GmbH & Co. KGaA, Weinheim